OCTOBER 25 2002

Experimental studies of a drumlike silencer

Y. S. Choy; Lixi Huang

J. Acoust. Soc. Am. 112, 2026–2035 (2002)
https://doi.org/10.1121/1.1508779

Experimental studies of a drumlike silencer

Y. S. Choy and Lixi Huang[a)]
Department of Mechanical Engineering, The Hong Kong Polytechnic University, Kowloon, Hong Kong

(Received 26 January 2002; revised 15 July 2002; accepted 15 July 2002)

The theoretical finding of the broadband performance of a reactive silencer is validated experimentally. The silencer consists of two highly stretched membranes lining part of the duct and backed by two long and shallow cavities. The test rig was built with a small square duct of 5 cm in dimension, and each cavity is 5 cm deep and 25 cm long. Two types of metal foils, stainless steel and copper, were used, and the lowest membrane-to-air mass ratio was 1.3. A transmission loss in excess of 10 dB was achieved over more than one octave band. For one configuration close to the optimal parameters, the predicted ratio of the frequency band limits is 2.47, while the experiment gave 2.35. Three spectral peaks were found in the stopband, as predicted, but the peaks were broader than prediction, indicating the presence of significant sound energy dissipation mechanisms. Comparison with theoretical simulation shows that the cavity damping dominates over membrane friction. Tests using heavier membranes and membrane with different levels of tension also agree with predictions. Issues of practical implementation of the concept as a flow-through silencer are also addressed. [DOI: 10.1121/1.1508779]

PACS numbers: 43.50.Gf, 43.20.Tb, 43.20.Ks [MRS]

I. INTRODUCTION

In a recent theoretical study, the second author explored the use of tensioned membranes as a sound reflection device with zero pressure loss penalty in a flow duct (Huang, 1999). In that study, the effect of air external to the membrane, which forms part of the duct wall, was excluded. In order to explore the use of the concept in a real silencer, a cavity has to be added to prevent the noise break-out. The formulation has since been extended to include the important cavity effect. Preliminary tests were carried out by the first author to validate the theoretical framework (Choy, 2001). With further refinement on the prediction, it now becomes clear that far better results are possible with membranes stretched far beyond the elastic limit of the plastic material used in those initial tests. The present paper reports the full comparison between the latest prediction and the tests using metal foils as membranes. The performance of these metal foils is comparable with that in many related studies, which are very briefly reviewed below in the wider context of low-frequency noise control.

Low-frequency sound radiation often carries most of the sound power in many engineering applications, such as the ventilation fans and the vibrating machinery. In general, the thickness of sound absorption material required in noise control engineering is tied to the wavelength. Effective absorption of low-frequency noise is impractical in most circumstances. Before the discussion can be extended to reactive and active noise control methods, it is necessary to specify the circumstances of the noise problem. In the area of room acoustics, in which sound strikes the walls with normal or random incidence, a few effective treatments have been developed, such as Helmholtz resonator and membrane, or plate, absorbers. Helmholtz resonators have been used to enhance low-frequency noise absorption since, perhaps, very long time ago in human history (Brüel, 1951). Recently, the principle of Helmholtz resonator is again becoming essential as the microperforated (submillimeter holes) noise absorption techniques (Maa, 1975, 1998) are being rapidly developed to offer fiberless and relatively broadband solutions (Zha *et al.*, 2002) for broadcasting studios, music and concert halls. Theoretical studies in this area have also increased in their sophistication, e.g., Brown, 1964; Ford, 1969; Sakagami *et al.*, 1996; Kang and Fuchs, 1999; and Horoshenkov and Sakagami, 2001. In its simplest setup, a panel absorber is a mass-spring system in which the mass derives from the panel, and the stiffness is mainly determined by the air cavity although the panel may also have a significant contribution. A shallow cavity gives high stiffness, and this is one of the main reasons why low-frequency, broadband noise is difficult to deal with. In this regard, the concept of magnetic field neutralizing the cavity air stiffness introduced by Huang (2000) could be a potential source of advancement in this field.

In the area of duct noise control, absorption of low-frequency noise by duct lining is more difficult than in rooms due to the grazing incidence in duct. Effective noise control is achieved with intrusive devices, such as a splitter silencer, or normal vehicle silencers in which the air flow passage is tortuous. But there are many important utilities, such as power plant chimneys and central ventilation systems, where the pressure loss caused by such a design means a substantial running cost. One alternative to achieving low-frequency noise abatement in a duct is the active noise control technique. Despite the rapid development in this field in the last few decades, successful applications of this old concept are still few. Apart from many electronic intricacies, the ineffectiveness of the secondary sound source at low frequencies may also be a factor.

The group led by Fuchs (2001) have been in the forefront of taming the low-frequency noise without imposing

[a)]Author to whom correspondence should be addressed. Electronic mail: mmlhuang@polyu.edu.hk

much pressure loss penalty. Among many patents they have developed, two are particularly relevant to the present studies. One is called the membrane absorber box, as described in detail by Ackermann, Fuchs, and Rambausek (1988), and the other is called the 'cleanable reactive silencer' [see Zha *et al.* (2002) for a brief scientific discussion]. The latter essentially looks like an expansion chamber except that the smaller tube runs all the way through the chamber with a small perforated segment immediately downstream of the first junction. The device is reactive, similar to the drumlike silencer described in the present study, but the insertion loss spectrum is typical of a resonator, which is what it essentially is. The biggest advantage here is that there is no pressure loss with this design, and the disadvantage is that many such silencers have to be installed in a row to achieve a broadband performance.

The device of membrane absorber box is a dissipative one with a broadband performance in the low to medium frequency range. It is made by a host of combined Helmholtz and panel resonators in a honeycomb structure. A typical resonator unit consists of a hollow rectangular cavity covered by a perforated membrane. Another impervious thin membrane is placed in front of the perforated membrane to form a narrow channel between the two sheets. The system of perforated panel with cavity resonates at a frequency about twice the resonant frequency of the Helmholtz system formed by the cavity and the aperture. The two resonances are only weakly coupled. Without the impervious membrane cover, the effect of the combined resonator would be rather poor as the spectrum of each resonator is peaky. But the narrow channel between the two sheets helps to increase the system resistance and the dip in the sound absorption spectrum is reduced. The details of the unit impedance are described in Frommhold *et al.* (1994). A splitter silencer built on this concept was successfully used in the exhaust stack of a papermill (Ackerman and Fuchs, 1989). The duct was 1 m wide and the silencer was 1 m long. Each splitter is 100 mm thick and the distance between adjacent splitters is 150 mm. An insertion loss of 10 dB or above was achieved over one octave band starting from 175 Hz. The device is mainly absorptive although some reactive mechanism might also be at work. This contrasts with the entirely reactive mechanism of the drumlike silencer being explored in the current study. This difference aside, two parallels can still be drawn. One is that the two devices share exactly the same goal of low to medium frequency duct noise abatement, and the other is that both achieve a stopband wider than one octave.

The current paper compares the experimental data of the drumlike silencer, henceforth drum silencer, with the predicted performance. The theory necessary for prediction is outlined very briefly in the next section, followed by the description of the experimental rig. The optimal result obtained in the tests is then analyzed in terms of both transmission loss and energy loss mechanisms. The effects of membrane mass and tension are discussed towards the end.

II. THEORETICAL OUTLINE

As shown in Fig. 1, the theoretical model resembles a standard, two-dimensional expansion chamber with a main

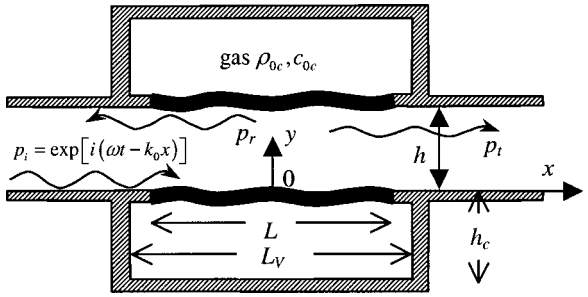

FIG. 1. Theoretical model of sound incident on two identical stretched membranes each backed by a cavity filled with a fluid which may differ from air.

channel height of h, and two identical cavities of length L_v and depth h_c. Two membranes are used to cover the two cavities, and their length can be less than that of the cavities, $L \leqslant L_v$. With the membrane cover, the gas medium inside the cavities can differ from air, and the gas density and speed of sound are denoted as ρ_{0c}, c_{0c}, respectively. The membranes have a mass per unit length m and a tensile force of T is applied. The basic method of transmission loss prediction follows that of an earlier study (Huang, 1999) in which the effect of the cavity air was ignored. In addition, the fluid inside the cavity in the present model is allowed to differ from that of air in the main duct. The need of doing so arises from the experimental finding (see Sec. IV) that there is a substantial amount of sound energy absorption inside the cavity.

When a harmonic sound of time dependence $e^{i\omega t}$ is incident on the membrane, it responds by vibrating at a velocity V which gives rise to a pressure difference Δp, for which the positive value denotes the downward action, hence fluid loading. This loading is borne by the membrane in addition to the incident wave perturbation, $p_i = e^{i(\omega t - k_0 x)}$, where $k_0 = \omega/c_0$ is the wave number and c_0 is the speed of sound in air. The dynamics of the fluid-structural coupling is described by the following equation for the displacement calculated as $\eta = V/(i\omega)$,

$$m\partial^2\eta/\partial t^2 - T(1+i\sigma)\partial^2\eta/\partial x^2 + \Delta p + p_i = 0, \tag{1}$$

where σ is a dimensionless loss factor of the membrane. The choice of this particular form of friction force is based on the following considerations. The usual dash-pot model would result in an inertia term like $m(1-i\sigma)\partial^2\eta/\partial t^2$. This implies that the tensioned membrane experiences friction even when it undergoes a uniform heaving motion, which we argue is not proper. Having said that, the physics of the real damping mechanisms in a thin tensioned membrane is rather complicated and is beyond the scope of current studies. Equation (1) is an *ad hoc* attempt to relate the energy loss with the shearing motion of membrane, and as such, σ is not necessarily identical to the loss factor normally quoted for materials, but the latter can be used as a reference. In fact, there are other acoustic loss mechanisms involved in the experimental rig, and more discussions on the modeling of the lumped energy loss are given later. The main objective of the current model is to provide some measure of accounting for the total vibration energy loss, so that the behavior of the

major part of sound power, which is shown to be reflected, may be better predicted. Comparison with the dash-pot model with the same σ shows little quantitative difference except that the dash-pot model gives very low damping at low frequencies while the current model gives more uniform loss throughout the spectrum.

The Galerkin procedure can be followed to solve Eq. (1) in terms of the modal expansion for a simply supported membrane,

$$V=\sum_{j=1}^{\infty} V_j \sin(j\pi\xi), \quad V_j=2\int_0^1 V\sin(j\pi\xi)d\xi, \quad \xi=x/L+1/2. \tag{2}$$

The main task in doing so is to relate the fluid loading Δp with the vibration velocity V through a modal impedance matrix $\{Z_{jl}\}$ as shown below,

$$\Delta p=\sum_{l=1}^{\infty}\left(\sum_{j=1}^{\infty} V_j Z_{jl}\right)\sin(l\pi\xi), \tag{3}$$

where the single mode impedance Z_{jl} is defined as the lth fluid loading coefficient caused by the vibration of the jth *in vacuo* mode of unit amplitude, $\sin(j\pi\xi)$. Substitution of Eq. (3) into Eq. (1) then forms a set of linear equations for the vibration velocity coefficients V_j, $j=1,2,3,...$, which may be truncated to an order like $j=N=25$, and solved by standard matrix inversion techniques like Gaussian elimination.

The task of finding the modal impedance Z_{jl} is one in which, unlike the coupled membrane dynamics, the membrane vibration is specified, and the loading is customarily called the radiation pressure. The radiation pressure on the membrane surface facing the main duct, denoted as $p_{+\mathrm{rad}}$, can be found by the summation over all duct acoustics modes, ψ_n, as shown below (see, for example, Doak, 1973):

$$p_{+\mathrm{rad}}(x,y,t)=\frac{\rho_0}{2h}\sum_{n=0}^{\infty} c_n\psi_n(y/h)\int_{-L/2}^{+L/2}\psi_n(y'/h) \times V(x',y',t)[H(x-x')e^{-ik_n(x-x')} + H(x'-x)e^{+ik_n(x-x')}]dx',$$

$$\psi_n(y/h)=\sqrt{2-\delta_{0n}}\cos(n\pi y/h), \quad k_n=\frac{\omega}{c_n}, \quad c_n=\frac{ic_0}{\sqrt{(n\pi/k_0h)^2-1}}, \tag{4}$$

where ρ_0 is the air density, c_n and k_n are, respectively, the phase speed and wave number of the nth duct mode, H is the Heaviside function, δ_{0n} is the Kronecker delta. The integration is carried out over the source surface: $x'\in[-L/2,L/2]$, $y'=0$. This result can be easily adapted for finding the radiation pressure in the lower (cavity) channel, denoted as $p_{-\mathrm{rad}}$, when ρ_0 and c_0 are replaced by the corresponding medium properties inside the cavity, ρ_{0c} and c_{0c}, respectively, the vibration velocity V replaced by $-V$, and h replaced by h_c. Sound reflection by the cavity walls at $x=\pm L_v/2$, denoted as $p_{-\mathrm{ref}}$, is also expressed as a summation of duct acoustics modes ψ_n like in Eq. (4) except that the two Heaviside functions are replaced by two constants, A and B,

$$p_{-\mathrm{ref}}(x,y,t)=\frac{\rho_{0c}}{2h_c}\sum_{n=0}^{\infty} c_{nc}\psi_n(y/h_c)\int_{-L/2}^{+L/2}\psi_n(y'/h_c) \times[-V(x',y',t)] \times[Ae^{-ik_{nc}(x-x')}+Be^{+ik_{nc}(x-x')}]dx',$$

$$c_{nc}=\frac{ic_{0c}}{\sqrt{(n\pi/k_{0c}h_c)^2-1}}, \quad k_{nc}=\frac{\omega}{c_{nc}}, \tag{5}$$

which are found by the rigid wall boundary conditions at $x=\pm L_v/2$,

$$\left.\frac{\partial(p_{-\mathrm{rad}}+p_{-\mathrm{ref}})}{\partial x}\right|_{x=\pm L_v/2}=0\rightarrow A=\frac{e^{ik_{nc}(L_v-2x')}+1}{e^{ik_{nc}(2L_v)}-1}, \quad B=\frac{e^{ik_{nc}(L_v+2x')}+1}{e^{ik_{nc}(2L_v)}-1}. \tag{6}$$

Both ρ_{0c} and c_{0c} can be complex quantities if sound absorption material is used and modelled as an equivalent fluid, in which case both are functions of frequency. In the next section, mechanisms of cavity energy dissipation is modelled by such an approach using the properties of glass-fiber of various porosity.

Once the vibration velocity is found via modal coefficients V_j through solving the coupled dynamics equation, Eq. (1), the reflected wave, denoted as p_r, can be found by evaluating the radiated wave into the far left from Eq. (4), while the transmitted wave, p_t, is found by the superposition of the incident wave, p_i, with the radiation into the far-right. The coefficients of energy flux reflection, β, wave absorption, α, and the transmission loss, TL can be evaluated as follows:

$$p_r=p_{+\mathrm{rad}}|_{x\rightarrow-\infty}, \quad p_t=p_{+\mathrm{rad}}|_{x\rightarrow+\infty}+p_i, \quad \beta=\left|\frac{p_r}{p_i}\right|^2, \quad \alpha=1-\beta-\left|\frac{p_t}{p_i}\right|^2, \quad \mathrm{TL}=20\log_{10}\left|\frac{p_i}{p_t}\right|. \tag{7}$$

The theory can be checked by the calculation of sound reflection by a simple expansion chamber without membranes by allowing the membrane mass and tension to vanish. This is described in the next section, and the result is compared with experimental data for the expansion chamber, a step which also helps to check the experimental method.

III. EXPERIMENTAL SETUP

As shown in Fig. 2, the transmission loss across the drum silencer is measured by the four-microphone, two-load method similar to the one described by Munjal and Doige (1990), and the resolution of the standing wave pattern follows the principle described by Chung and Blaser (1980). Briefly, two microphones are required to resolve the two travelling waves in a standing wave pattern. The theoretical definition of transmission loss involves a downstream condition which is anechoic. This is not normally possible without using excessively long duct lining for low frequencies.

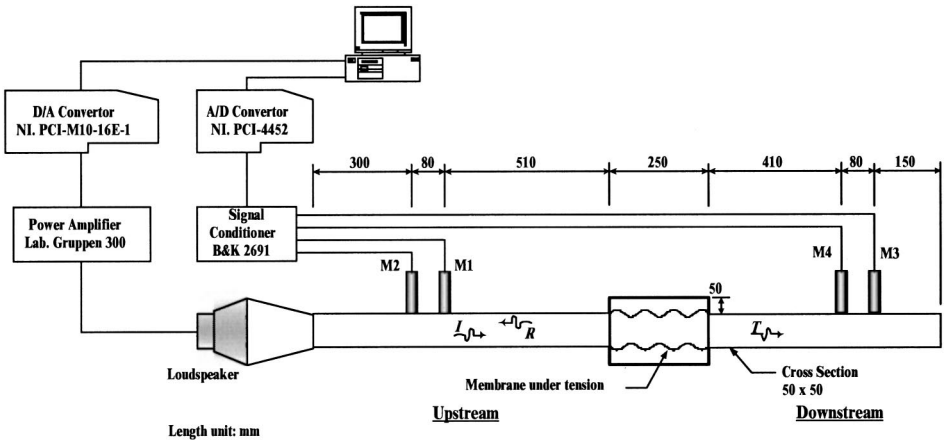

FIG. 2. The four-microphone, two-load measurement system. Both data acquisition and source sound generation are controlled a Labview code in a computer equipped with A/D and D/A cards.

Therefore the wave pattern downstream of the muffler remains a standing wave. A total of four microphones are needed for the simultaneous measurements of the two standing wave patterns, one upstream and one downstream. Even this is insufficient to define the transmission loss since the downstream segment still has reflection wave, say $R_{d1}e^{i(\omega t+kx)}$. It is possible, and indeed necessary, to change the configuration at the downstream without affecting the muffler itself, so that a different standing wave pattern is created and measured giving another residual reflection wave $R_{d2}e^{i(\omega t+kx)}$. The linear combination of the two sets of data forms another set which is acoustically correct for the muffler. The combination can be done in such a way that $R_{d1}+\varphi R_{d2}=0$, i.e., the downstream becomes anechoic. φ is a complex constant which is determined experimentally by this anechoic requirement. The derived data set is non-trivial only when the two actual experiments are linearly independent of each other, i.e., when they are conducted with different downstream impedance conditions. The magnitudes of the incident and transmitted waves in the derived data set can be determined by the same combination constant φ and the transmission loss is found.

The incident noise is simulated by a loudspeaker connected to the duct through a contraction cone. A digital-to-analogue conversion card (PCI-M10-16E-1 from National Instruments) is used to generate the signal which is amplified by one of B&K's amplifiers (Lab Gruppen 300). Two pairs of 1/2 inch, phase-matched microphones (B&K type 4187) are used together with conditioning amplifier (B&K's Nexus 2691). The separation distance for each pair is 8 cm. The large separation is chosen to reduce experimental error at low frequencies up to 1500 Hz. Signals from the four microphones, labeled M1 through M4, are digitized by the National Instruments card PCI-4452 at the sufficient sampling rate of 16 KHz. Both A/D and D/A processes are controlled by National Instruments' Labview program and the test is run by a loop of discrete frequencies from 20 Hz to 1.5 kHz with a 10 Hz increment. The discrete frequency approach is preferred since it offers opportunities to adjust the loudspeaker volume at nodal frequencies where the output can be very low. Since the frequency of the incident wave is accurately controlled by the Labview program, the length of each sample can be tailor-made to be an integer number of cycles, eliminating any possible spectral leakage through the use of digital windowing technique. The program can also be run with random noise measurement, but it is felt that the time required to scan through the whole frequency spectrum is acceptable thanks to the automatic looping function of the Labview code.

The exact locations of the microphones are shown in Fig. 2 with the length unit of mm. Before the two-load tests are conducted, microphones M2, M3, and M4 are calibrated against M1 by the swapping procedure despite the fact that all microphones are very well phase matched. The resultant variations of the amplitude ratio and phase angle difference with respect to frequency are fit to a polynomial curve and saved in files to be read by the Labview code which runs the two-load tests. The first test is conducted with the far end of the downstream section filled with some sound absorption materials providing a partially anechoic termination. The second test is conducted without any sound absorption material. In both tests, the far downstream end is terminated by a rigid plate so that the signal will not be contaminated by the background noise. The rigid end and partially anechoic end conditions provide two linearly independent tests as required by the two-load method.

The duct used in the tests has a square cross section of dimension $h=5$ cm. The two cavities also have the nominal cross section of 5 cm by 5 cm and the length is 25 cm. These dimensions can be adjusted by adding or retrieving some solid blocks in the rig. The first cut-on frequency in the rigid duct is 3430 Hz. According to the prediction, the lower limit of the stopband frequency may be down to a dimensionless frequency of $fh/c=0.05$ or $f=343$ Hz. Such a frequency is not that low in the usual sense, but the general agreement reached between the experimental data and the theoretical prediction gives reasonable confidence that substantial noise reflection at frequencies below 100 Hz can be achieved for a duct with a height of 20 cm or so. The choice of the 5 cm duct in this experiment is partly based on the convenience of an existing rig. In contrast, the choice of the relatively large separation distances between the two junctions of the chamber housing the silencer and the nearest microphones is forced upon by the inconvenience of accommodating the external device required to apply and change the membrane tension. Account is taken of the acoustic damping by the duct walls according to the well-known formula of complex wave numbers (see Pierce 1991, Eqs. 10-5.10 and 10-5.8):

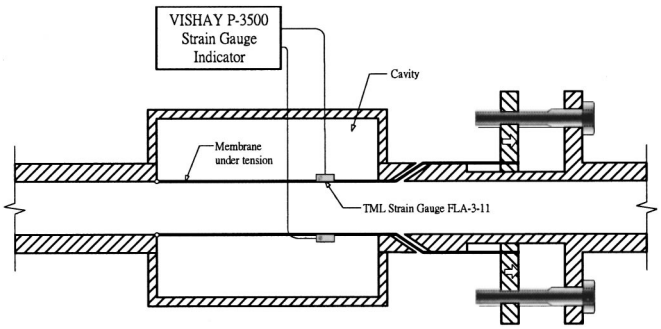

FIG. 3. The mechanism to apply and measure the membrane tension.

$$k=\frac{\omega}{c_0}+(1+i)\alpha_{\text{walls}},$$
$$\alpha_{\text{walls}}=2^{-3/2}\sqrt{\frac{\omega\mu}{\rho_0 c_0^2}}\left[1+\frac{\gamma-1}{\text{Pr}^{1/2}}\right]\frac{L_p}{A}, \tag{8}$$

where μ is the air viscosity, γ is the ratio of specific heats, Pr the Prandtl number, L_p the perimeter, and A the cross sectional area. The energy loss has a square-root frequency dependency. Take 500 Hz as an example, friction for the present duct over 1 m gives around 5% loss in sound energy flux. Corrections for travelling wave amplitudes are made by finding out the true incident and reflection waves at the left-hand side junction of the chamber from the sound intensities measured between M1 and M2. The same applies to the downstream. But the effect of friction inside the chamber is regarded as part of the damping mechanism of the silencer. No attempt is made to separate friction from other mechanisms such as the inevitable vibration of the so-called rigid walls of the cavity.

The membranes are clamped and stretched by a mechanism shown in Fig. 3. The upstream end of the membrane is simply fixed by wrapping it around a cylinder of 6 mm in diameter and pressed against the junction walls. The downstream end of the membrane runs through a 0.05 mm slit, which is exaggerated in the figure, to be fixed by two plates outside the duct. The axial positions of these clamp plates, hence the strain in the membrane, are easily adjusted by the screws shown in the figure. The tensile force applied is measured by a strain gauge glued to the surface of the membrane in the test section. The dimension of the strain gauge sensor (TML FLA-3-11) is 3 mm and its attachment is believed to cause no noticeable influence on the dynamics of the stretched membrane. However, since the membrane used is thinner than the epoxy used to attach the strain gauge, significant measurement uncertainties may occur. To eradicate this problem, a calibration procedure is undertaken by attaching dead weights to the membrane through some connection joints in the upright position.

In the direction perpendicular to the figure, say, z, the two edges of the membranes (of width 52 mm) are inserted into a very thin gap between the two constituent plates of the cavity walls. The gap is less than 0.5 mm and has a depth around 1–2 mm in the z direction. This is a deliberate attempt to simulate the two-dimensional theoretical model shown in Fig. 1. Tests were also conducted using a membrane narrower than 50 mm leaving a small gap between the membrane edges and the end walls, but results were quite similar. It is anticipated that, in real applications, the edges of tensioned membranes should be entirely glued to the end walls, for which a three-dimensional theoretical model should be developed.

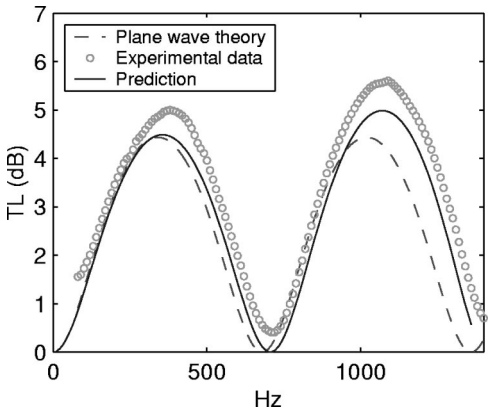

FIG. 4. Comparison of the measured data with predictions by the plane wave approximation and the modal expansion calculation with zero membrane mass and tension.

When the membranes are removed and the slit allowing the membranes to get out of the duct is covered, the rig becomes a simple expansion chamber with an area expansion ratio of 3. The transmission loss is measured and compared with two theoretical predictions in Fig. 4. One is the plane-wave theory (dashed line), and the other is the present theory using 25 modes of the virtual membranes (solid line). It is found that the comparison between the experimental data with the present theory is better than that with the plane-wave approximation. The latter ignores the acoustic scattering at the junctions leading to two characteristic differences with reality. In reality, the frequency range of the lobes of the transmission loss is larger than $c_0/2L$, and the peak transmission loss is higher than that determined by the plane-wave theory. These are all captured correctly by the present theory. Having said that, the measured transmission loss is typically 0.5 dB higher than the theoretical prediction. This is probably caused by some energy dissipation mechanisms which are necessarily present in the rig but excluded in the theory. Apart from the damping by the sharp edges, such as the 6 mm cylinder used to clamp the membranes, one possible mechanism is the vibration of many constituent parts of the rig which is required to adjust the cavity size during the experimental study. When the same measurement system and procedure were used earlier in a single-piece circular expansion chamber, the discrepancy between the experimental data and the prediction using a finite element calculation was reduced to 0.2 dB at the nodal frequencies of the transmission loss lobes. Despite the finite discrepancy between the prediction and the experimental data, the test of the expansion chamber serves as a mini validation for both experimental setup and the theory.

IV. BASIC ANALYSIS

According to the theoretical prediction, the membrane mass has adverse effect on the silencer performance. Two

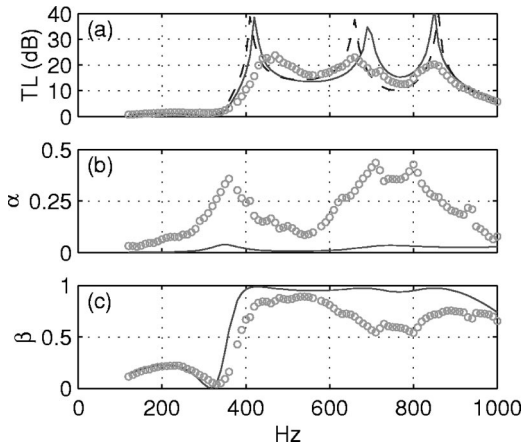

FIG. 5. Comparison of experimental data with theoretical predictions for (a) transmission loss TL, (b) absorption coefficient α, and (c) reflection coefficient β. The experimental data (open circles) was obtained for the thin stainless steel under 190N tension. The predictions were for the same membranes with a loss factor of $\sigma=0.5\%$ under tension 190N (solid lines) and 181N [dashed line in (a)].

types of metal foils were available at the time of experiment: stainless steel and copper. The stainless steel foils were 0.01 mm and 0.02 mm thick. The membrane is weighed, and the mass ratio for the thinner one is calculated as follows:

$$m_1=\frac{m}{\rho_0 h}=\frac{7800\times 0.01}{1.225\times 50}=1.3. \tag{9}$$

This is sufficiently low although even lower values can be achieved by using aluminum foil in a larger duct. This section focuses on the best result using this foil, leaving the results for heavier membranes and the effect of tensile force to the next section.

Here, the stopband is defined as the frequency range, $f\in[f_1,f_2]$, in which the transmission loss is everywhere equal to or higher than 10 dB, a level which is much higher than the peak performance of around 5 dB for an empty expansion chamber with an area ratio of 3. Based on the mass ratio of $m_1=1.3$, and assuming a membrane loss factor of $\sigma=0.5\%$ for stainless steel, an optimization calculation can be conducted to see what tension T would yield the highest bandwidth represented by f_2/f_1. The result is shown below in dimensionless form first,

$$\begin{aligned} &f_1 h/c_0=0.0548, \quad f_2 h/c_0=0.1378,\\ &f_2/f_1=2.516, \quad T_{\mathrm{opt}}/(\rho_0 c_0^2 h^2)=0.502. \end{aligned} \tag{10}$$

The predicted dimensional optimal tension, T_{opt} and band frequencies for the particular rig are given below,

$$f_1=377\ \mathrm{Hz}, \quad f_2=947\ \mathrm{Hz},$$

$$T_{\mathrm{opt}}=0.502\times 1.225\times(343\times 0.05)^2=181\mathrm{N}.$$

This prediction is shown in Fig. 5(a) as the dashed line. Three peaks are found and the dip between the second and third peaks is right on the critical level of 10 dB. Study of the variation around this tension shows that the dip goes below 10 dB for a slightly lower tension, indicating that the tension does play a very subtle role in setting the frequency intervals between the spectral peaks. The dip remains above 10 dB for higher tension but the stopband of TL$>$10 dB is slightly narrower. In the experiments, tensions were applied with an increment of 10N, and the stopband of 190N was found to be wider than that of 180N. So, the experimental data of 190N is chosen for analysis. In Fig. 5, the experimental data is shown in small open circles and the prediction for 190N is shown as solid curves.

As shown in Fig. 5(a), the predicted stopband is $f\in[385,953]$ Hz, while the experimental result is $f\in[398,935]$ Hz. The ratio of frequency limits, f_2/f_1, are 2.47 and 2.35, respectively. Figure 5(b) compares the sound absorption coefficient, α, and Fig. 5(c) shows the reflection coefficient of sound energy flux, β. The following observations are made.

(1) In agreement with the prediction, there are three distinct spectral peaks found within the experimental stopband. This means that the basic theoretical model is correct for the experimental rig.
(2) The predicted TL curve has sharp peaks while that from the experiment is smoother. It means that there are significant energy dissipation mechanisms in the rig which are excluded from the theory. The experimental value of α ranges from 10% to 45% within the stopband, which is roughly 10 times higher than the predicted value with $\sigma=0.5\%$.
(3) Also in agreement with theory, the experimental data shows that the mechanism of sound reflection dominates over sound absorption in the whole experimental stopband. As shown in Fig. 5(c), the prediction agrees with the experimental data almost perfectly below 300 Hz, which constituents the first small lobe.

In order to make a proper account of the sound energy damping in the rig, four possible mechanisms are suggested,

(1) membrane damping over the bulk vibrating surface;
(2) membrane damping at the edges;
(3) cavity damping; and
(4) sound induced vibration of some walls during the low frequency test.

Since the membrane is so thin and the dynamics of air and structure are fully coupled, it is impossible to separate mechanisms (1) from (3). The identifications of mechanisms of (2) and (4) are also difficult. Two models are proposed below, one for mechanisms (1) and (2), and another for (3) and (4).

It might be assumed that mechanism (2) dominates over mechanism (1). The losses concentrated at the leading and trailing edges of the membrane should be described by delta functions, $\delta(|x\pm L/2|)$, but the fact that there are two other edges in the membrane length direction gives some hope that a model of distributed energy loss might at least capture some essential characteristics of mechanisms (1) and (2). This is done by assigning an equivalent material loss factor σ which should be much higher than 0.5%, the typical value listed in material handbooks for metals. This model is called the σ model.

Cavity damping, mechanism (3), is again hard to model

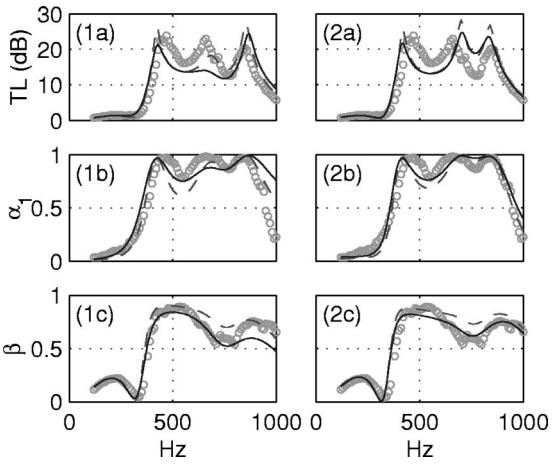

FIG. 6. Modeling of damping mechanisms by two methods: equivalent membrane loss factor (1a), (1b), and (1c), and equivalent sound absorption material in the cavities (2a), (2b), and (2c). The experimental data are shown in open circles, and two levels of damping mechanisms are calculated in each model. In the left column, σ is 5% for the dashed lines, and 10% for the solid lines. In the right column, R_{sam} is 40 kg/m^3 s for the dashed lines and 80 kg/m^3 s for the solid lines.

exactly. Usually, a loss coefficient is assigned to each cavity mode. This procedure becomes awkward in the present model using the expansion of membrane vibration in terms of the *in vacuo* modes of the simply supported membrane. It is assumed that the combined effects of mechanisms (3) and (4) may be modeled by treating the empty cavity as one filled with a very fluffy sound absorption material. This is done by assigning a small value of flow resistivity R_{sam} and the model is labeled as the sam model. Once R_{sam} is given, the complex density and speed of sound in the cavity, ρ_{0c}, c_{0c}, can be specified as functions of frequency and flow resistivity (or porosity) using empirical properties of common materials like fiberglass available in Mechel and Vér (1992).

Going back to Figs. 5(b) and (c), it is observed that high sound absorption rate occurs when the reflection coefficient is low. A more useful comparative study can be made by the relative sound absorption coefficient

$$\alpha_1 = \alpha/(1-\beta), \tag{11}$$

which is a more sensible measure of how much noise that actually enters the silencer is absorbed. Using this concept, the effects of σ and R_{sam} are studied separately, and the results are shown in Fig. 6. The subfigures on the left-hand-side columns are for the σ model, while those on the right-hand side are for the sam model. For each model, two levels of losses are tested. The dashed lines are for the lower levels and the solid lines higher values. The two levels are chosen in such a way that the experimental data for 190N (open circles) generally fall within the range predicted by the two levels with a heuristic curve-fitting. As shown in Fig. 6(1b), the comparison between the experimental data and the result of the level 1 loss factor σ=5% shows a large deficit of relative damping (α_1) around 540 Hz. This discrepancy is reduced by the level 2 model with $\sigma=10\%$. But, as shown in Fig. 6(1a), the transmission loss of the two predicted falls below the experimental value due to the inability to simultaneously predict the correct reflection coefficient in this region, as shown in Fig. 6(1c). The modelling of the spectral dip around 775 Hz and the third peak around 855 Hz is more successful, but that for the second peak around 670 Hz is not. The transmission loss for $\sigma=5\%$ retains a distinct peak, but it overpredicts the reflection. The model of $\sigma=10\%$, on the other hand, simulates β correctly but the TL peak disappears due to the lack of sufficient membrane response. However, assigning a lower value of σ for the first mode does not yield a better overall agreement with the experimental data. These tests, together with the fact that the frequencies of TL peaks are not predicted accurately, seems to suggest that some three-dimensional effects inherent in the experiment is responsible for the discrepancy between the data and the two-dimensional theoretical model. These include the possible corrugation of the membrane when it's slightly twisted during the application of tensile force, nonuniformity of the tensile force across the width in the z direction, and the possible effect of the gap between the membrane edges and the duct walls along the axial direction, etc. There are also other factors in the rig which are normally excluded in any theoretical model. For example, the effect of the attachment of the strain gauge is believed to be minor but, admittedly, it is hard to assess this accurately.

The sam-model based on the fiberglass properties is tested for two levels of flow resistivity, $R_{\text{sam}}=40$, 80 kg/m^3 s, which are about three orders of magnitude lower than that used in usual duct linings. The results are shown in the right-hand-side column of Fig. 6. Figure 6(2b) shows that the level 1 model underpredicts the loss around the first spectral dip at 540 Hz but, contrary to the σ models, sam models of both levels overpredict the loss around the second spectral peak at 685 Hz. The match between the sam model and the experimental data is very good beyond the third spectral peak for both α_1 and β. Figure 6(2a) shows that three spectral peaks are simulated with satisfactory sharpness although, like the essentially lossless model shown in Fig. 5(a), the interval between the second and third peaks is narrower than the experimental result. The overall conclusion is that the sam model simulates better than the σ model, and an intermediate level of $R_{\text{sam}}=60$ kg/m^3 s will be used with the basic material loss factor of σ=0.5% in all subsequent comparative studies between theory and experiment.

V. EFFECT OF MEMBRANE PROPERTIES

The variation of transmission loss spectrum with respect to the membrane tension is shown in Fig. 7 for the thin stainless steel foil ($m_1=1.3$). Four spectra for 110, 180, 190, and 200N are chosen for display. The experimental results (open circles) are compared with the theoretical modeling (solid lines) with $R_{\text{sam}}=60$ kg/m^3 s, and $\sigma=0.5\%$. Figure 7(a) is for the tension of 110N. This is a typical situation where there are only two peaks in the stopband since the third one is too far away from the second. The theoretical modelling is seen to be rather successful except that the heights of all the peaks are over-estimated. Figure 7(b) is for 180N, which is shown earlier to be close to the theoretical optimal value of 181N. Although the second peak is rather close to the third, the breakdown between the two peaks is still too serious to qualify for a broadband performance un-

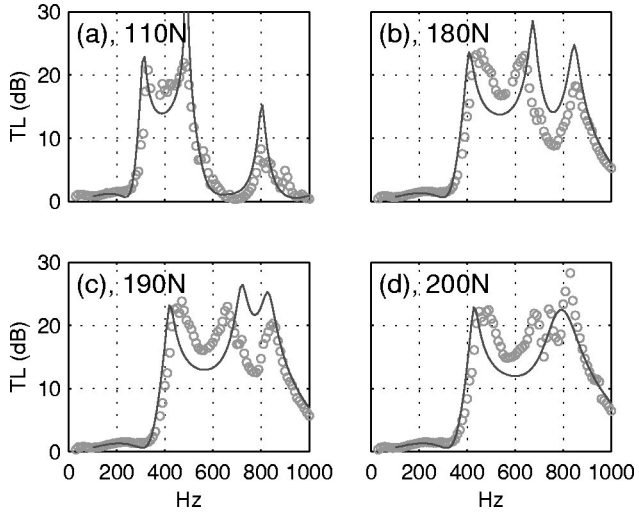

FIG. 7. Variation of TL spectrum with respect to tension for the thin stainless steel foil of $m_1=1.3$. The values of tension are labeled in subfigures. Open circles are the experimental data, and the solid lines are predictions incorporating a cavity damping model with $R_{\text{sam}}=60\ \text{kg/m}^3\ \text{s}$ and $\sigma=0.5\%$.

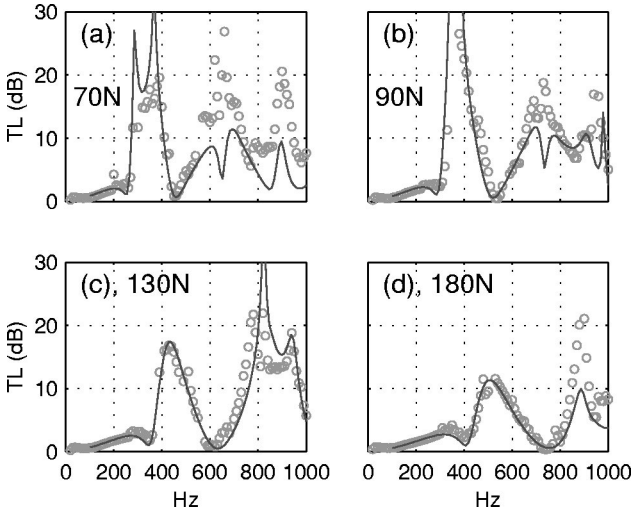

FIG. 8. The performance of a drum silencer made of copper foils of 0.03 mm thick and 198 mm long, with a 65 mm deep cavity. The open circles are the experimental data, and the solid curves are predictions using a cavity damping model with $R_{\text{sam}}=60\ \text{kg/m}^3\ \text{s}$ and $\sigma=0.5\%$.

der the strict criteria of TL$\geqslant$10 dB at all discrete frequencies. If one third octave band averaging is applied, as is done in most practical applications, this breakdown can be overlooked. The point to be emphasized here is that the spectral variation with respect to T is gradual in every sense, and the sudden change of the bandwidth with T is purely caused by the rigid definition of the stopband. The modelling in this case can also be regarded as being successful given the fact that the peak frequencies cannot really be determined accurately with a two-dimensional theory. Figure 7(c) is for 190N and is analyzed in detail earlier. Comparing with the experimental spectrum in Fig. 7(b), the interval between the second and the third peaks of the experimental data is reduced, leading to a more balanced picture with a wider stopband. This change of pattern is captured rather accurately despite the two-dimensional approximation. Figure 7(d) is for 200N in which the second and third peaks from the experiment seem to merge together. The merge is more complete in the theoretical prediction in this case, consistent with the overprediction of the second peak frequency in all previous cases.

Experiments using copper foil of thickness 0.03 mm were also conducted with less impressive results. This outcome is expected, but the results are also analyzed here to confirm the theoretical prediction of adverse effects of membrane mass. For this foil, the cavity was changed to a shorter and deeper one following the theoretical search for a reasonable performance for the heavy foil. The parameters are $h_c=65$ mm, $L_v=L=198$ mm, $m_1=4.43$. The results are compared with theoretical modeling in Fig. 8. Figure 8(a) is for the tensile force of 70N, and the data seems to be rather scattered relative to the theoretical modeling. The same phenomena are observed for tests with lower tension values such as 30N and 50N. This was found to be caused by the difficulty in setting up a uniform stress for the foil at such low tension. The agreement between theory and experiment becomes much improved for tests with higher tensile forces of 90N, 130N and 180N in Figs. 8(b), (c), and (d), respectively. Comparing the results from the lighter foil of stainless steel in Fig. 7, it is found that the heavier copper foil yields stopband in lower frequencies but the bandwidth is also narrower.

Since noise abatement at extremely low frequencies is difficult, it might be reasonable to adopt a performance criterion which varies somewhat with frequency. In that case, heavy metal foils with a medium stress level will be the most suitable choice. To demonstrate the effect of mass on spectrum, the typical result of the thin stainless steel foil shown in Fig. 7(c) is plotted together with that of the thick copper foil shown in Fig. 8(a) for comparison. These are presented as Figs. 9(a) and (c), respectively. A thicker stainless steel

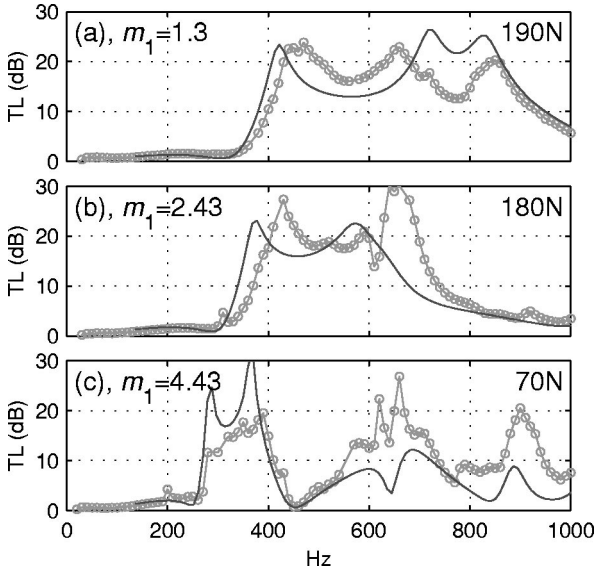

FIG. 9. Comparison of stopbands for three different values of membrane mass which is marked in each subfigure. (a) is the thin stainless steel with $L_v=L=25$ cm, $h_c=5$ cm. (b) is for a thicker stainless steel foil with a cavity length $L_v=30$ cm which is longer than the membrane length $L=25$ cm, while $h_c=5$ cm. (c) is copper foil with $L_v=L=198$ mm, $h_c=65$ mm.

foil was also tested. Its mass ratio of 2.43 provide the intermediate value, so the result is shown in Fig. 9(b). The general trend of spectral shifting towards lower frequencies is made clear. Notice that, for the thicker stainless steel foil shown in Fig. 9(b), the stopband is underpredicted, contrasting with all other comparisons.

VI. DISCUSSIONS

Several issues related to the actual implementation of the concept of drum silencer are discussed here based on what is learned from the two-dimensional modelling. The first issue is the significance of possible molecular relaxation of the stretched membrane after a period of use. For this purpose, the last test with the thicker stainless steel, shown in Fig. 9(b), was left in the laboratory for more than a week, and the reading for the tensile force was reduced from 180N to 178N, which is insignificant considering the accuracy of the strain gauge itself. The transmission loss was measured again and there was hardly any noticeable change. Strictly speaking, this test does not really simulate the actual situation where the silencer might be exposed to turbulent flow. For the moment, it can be said that the change of transmission loss spectrum with possible relaxation in tensile force is at least very gradual. The other related issue is acoustic fatigue. The stress level for this particular rig is around 380 MPa, which falls within the range of fatigue stress of carbon steels. In order to make sure that no fatigue occurs, good quality material should be chosen. But in actual application with larger duct, thicker membranes can be used, and the stress level comes down even with the same tensile force, so the choice of material should be plenty.

The second issue is the possibility of flow-induced vibration, and secondary sound radiation caused by this vibration. This issue should be divided into two parts. The first is the possibility of sound radiation by forced membrane vibrations due to turbulent flow eddies. The second is the possibility of self-induced vibration which would lead to a possible breakdown of the membrane, a problem much more serious than the noise itself. For the first part, reference can be made to the work of Ffowcs, Williams, and Hill (1987), who treated the problem of scattering of frozen, convective wave pattern within the boundary layer flow by abrupt changes in structural properties, which in the drum silencer is from the rigid wall to the tensioned membrane. Considering the small length scale of the turbulent eddies, see Howe and Baumann (1992), such transfer of energy from the near field to the far field is most likely to concentrate in the region of high frequencies. This possible problem of high frequency radiation is much less important than the low-frequency noise being addressed in the present study. For the second part, extensive studies have been carried out by the second author on this topic (Huang, 1998, 2001), and it can be concluded that it is unlikely that the membrane would experience any form of flutter (transfer of mean flow energy to growing structural vibration) when the flow speed is well below the *in-vacuo* tensile wave speed in the membrane. The latter is very high for the drum silencer studied here. Take the thin stainless membrane as an example,

$$c_T = \sqrt{\frac{T}{mh}} = \sqrt{\frac{190}{7800 \times (0.01 \times 10^{-3}) \times 0.05}} = 221 \text{ m/s}.$$

This speed is unlikely to be approached in ordinary ventilation systems. If the flow speed does approach such value, the acoustic impedance of the system would have been changed drastically. The tensile force of 190N may no longer be the optimal tension, and the whole device has to be redesigned. The problem of self-induced vibration should be more seriously considered if the drum silencer is to be used in a high-speed wind-tunnel.

The third issue is the effect of three-dimensional features in any realistic design of drum silencer. Most likely the membranes will have to be fixed on all the edges. If no tension is applied in the third dimension *z*, most conclusions reached in the two dimensional model might be preserved although the membrane motion would become considerably more complicated. Three-dimensional modelling will have to be developed to predict and design such realistic drum silencers. Further investigation is also needed to better identify and model the damping mechanisms.

VII. CONCLUSIONS

The general conclusion of this study is that the theoretical predictions of the broadband performance of the so-called drum silencer are validated by experimental data despite two major limitations of the theory. One is the two-dimensional nature of the theoretical model, and the other is the exclusion of the damping mechanisms which are difficult to describe quantitatively. The following are specific conclusions derived from various tests conducted.

(1) The frequency range. Due to the small duct size, the dimensional frequencies do not fall in the low frequency range, say below 200 Hz, in engineers' common sense, but the dimensionless frequency range does agree with the prediction. This gives the confidence that low-frequency broadband noise can be tackled by the new concept of drum silencer. The main feature of the broadband performance is that three peaks appear with suitable intervals such that the breakdown between adjacent peaks remain moderate.

(2) Mechanisms of energy dissipation. In the specific design of the validation experiments, there exists a significant source of energy dissipation at frequencies when reflection is less effective. The exact nature of such damping mechanisms has not been identified convincingly, but it appears from the limited attempts of modelling that the cavity damping is dominant. The other major source of damping may arise from the clamped membrane edges, and the two nominally free edges in the third dimension. When membrane damping is introduced in a distributed manner, the amount of damping required to match the measured overall sound absorption coefficient suppresses the second spectral peak which is definitely present in the experiment. Simulation of cavity damping by fluffy sound absorption material proves to be capable of preserving all three peaks.

(3) Dominance of reflection. Sound reflection dominates in every part of the stopband despite the fact that the dimensional frequency encountered in the small duct rig is relatively high. It is speculated that the significance of the unaccounted contribution from damping will be reduced if a larger duct is used.
(4) Effect of membrane mass. A light membrane is shown, both theoretically and experimentally, to yield better performance than its heavier counterparts, membrane of zero mass being the theoretical optimum. However, according to the present theory, an aluminum foil of thickness 0.05 mm or more can still provide a stopband wider than one octave in a duct of 20 cm in cross sectional dimension. This excludes the potential technical problems that might be encountered by using ultrathin membranes.
(5) Optimal membrane tension. The optimal tension is identified theoretically and proved rather accurately in the tests. The problem of possible material relaxation of stretched membrane was only investigated briefly by measuring the same rig again after one week. No detectable change in tension nor performance was found in this test. However, this does not exclude the possibility of membrane relaxation in all practical situations. At this junction, it is stressed that the actual performance of the drum silencer does not change with tension in any abrupt manner although the level of tension does play a delicate role of regulating the intervals between spectral peaks.
(6) Multiple drum silencer. Since the stopband frequencies can be manipulated by many variables such as mass and tension, it is theoretically possible to come up with a very broadband design with the sequential combination of drum silencers of different membrane properties. The most profitable design would be the combination of many narrower stopbands in the very low frequency range while that in the medium to high frequency range is better taken care of by normal duct lining covered by light membranes under low tension.
(7) Self-induced vibration and secondary radiation of noise. With a brief reference to the results of related studies, it was shown that a drum silencer is unlikely to experience self-induced vibration because the optimal tensile stress required should be normally very high. Of course, the level of stress should still be within the elastic limits of normal materials like steel or aluminum. The *in vacuo* flexural wave speed far exceeds the usual flow speed in a normal ventilation tunnel, hence no flutter.

ACKNOWLEDGMENT

The first author thanks the Hong Kong Polytechnic University for the Ph.D. studentship.

Ackermann, U., and Fuchs, H. V. (**1989**). ''Noise reduction in an exhaust stack of a papermill,'' Noise Control Eng. J. **33**, 57–60.
Brown, S. (**1964**). ''Acoustic design of broadcasting studios,'' J. Sound Vib. **1**, 239–257.
Brüel, P. V. (**1951**). *Sound Insulation and Room Acoustics* (Chapman and Hall, London).
Choy, Y. S. (**2001**). ''Experimental study of absorption and reflection of grazing sound by flexible panels,'' Proceedings of the 8th International Congress on Sound Vibration, Hong Kong, China, pp. 1003–1010.
Chung, J. Y., and Blaser, D. A. (**1980**). ''Transfer function method of measuring in-duct acoustic properties. I. Theory,'' J. Acoust. Soc. Am. **68**, 907–913.
Doak, P. E. (**1973**). ''Excitation, transmission and radiation of sound from source distributions in hard-walled ducts of finite length (I): the effects of duct cross-section geometry and source distribution space-time pattern,'' J. Sound Vib. **31**, 1–72.
Ford, R. D., and McCormick, M. A. (**1969**). ''Panel sound absorbers,'' J. Sound Vib. **10**, 411–423.
Frommhold, W., Fuchs, H. V., and Sheng, S. (**1994**). ''Acoustic performance of membrane absorbers,'' J. Sound Vib. **170**, 621–636.
Fuchs, H. V. (**2001**). ''Alternative fiberless absorbers—new tools and materials for noise control and acoustic comfort,'' Acustica **87**, 414–422.
Horoshenkov, K. V., and Sakagami, K. (**2001**). ''A method to calculate the acoustic response of a thin, baffled, simply supported poroelastic plate,'' J. Acoust. Soc. Am. **110**, 904–917.
Ffowcs Williams, J. E., and Hill, D. C. (**1987**). ''On the scattering of evanescent waves into sound,'' J. Fluid Mech. **184**, 101–121.
Howe, M. S., and Baumann, H. D. (**1992**). ''Noise of gas flows,'' in *Noise and Vibration Control Engineering: Principles and Applications*, edited by L. L. Beranek and I. L. Vér (Wiley, New York), Chap. 14.
Huang, L. (**1998**). ''Reversal of the Bernoulli effect and channel flutter,'' J. Fluids Struct. **12**, 131–151.
Huang, L. (**1999**). ''A theoretical study of duct noise control by flexible panels,'' J. Acoust. Soc. Am. **106**, 1801–1809.
Huang, L. (**2000**). ''A theory of reactive control of low-frequency duct noise,'' J. Sound Vib. **238**, 575–594.
Huang, L. (**2001**). ''Viscous flutter of a finite elastic membrane in Poiseuille flow,'' J. Fluids Struct. **15**, 1061–1088.
Kang, J., and Fuchs, H. V. (**1999**). ''Predicting the absorption of open weave textiles and micro-perforated membranes backed by an air space,'' J. Sound Vib. **220**, 905–920.
Maa, D.-Y. (**1975**). ''Theory and design of microperforated panel sound absorbing constructions,'' Sci. Sin. **18**, 55–71.
Maa, D.-Y. (**1998**). ''Potential of microperforated panel absorber,'' J. Acoust. Soc. Am. **104**, 2861–2866.
Mechel, F. P., and Vér, I. L. (**1992**). ''Sound absorbing materials and sound absorber,'' in *Noise and Vibration Control Engineering: Principles and Applications*, edited by L. L. Beranek and I. L. Vér (Wiley, New York), Chap. 8.
Munjal, M. L., and Doige, A. G. (**1990**). ''Theory of a two source-location method for direct experimental evaluation of the four-pole parameters of an aeroacoustic element,'' J. Sound Vib. **141**, 323–333.
Pierce, A. D. (**1991**). *Acoustics, An Introduction to its Physical Principles and Applications* (Acoustical Society of America, New York).
Sakagami, K., Kiyama, M., Morimoto, M., and Takahashi, D. (**1996**). ''Sound absorption of a cavity-backed membrane: a step towards design method for membrane-type absorber,'' Appl. Acoust. **49**, 237–247.
Zha, X., Fuchs, H. V., and Drotleff, H. (**2002**). ''Improving the acoustic working conditions for musicians in small spaces,'' Appl. Acoust. **63**, 203–221.